2

Design of the Multi-module Manipulator

Tommaso Ranzani, Iris de Falco, Matteo Cianchetti and Arianna Menciassi

The BioRobotics Institute, Scuola Superiore Sant'Anna, Pontedera (PI), Italy

Abstract

In Chapter 1 all the suitable technologies have been surveyed and a direct comparison underlined how fluidic technologies have the best characteristics to meet the application scenario. In particular, flexible fluidic actuators have been identified as the most promising technology for providing omnidirectional bending and elongation, while granular jamming can represent a valid solution to implement variable stiffness features. In this chapter, we report the design of the single module, the strategy for integrating more modules, the fabrication and characterization of a 2-module manipulator.

2.1 The Design of the Single Module

Each module of the manipulator has to be able to independently perform omnidirectional bending, elongation, and stiffening. This is possible thanks to two different actuation systems integrated in each module: flexible fluidic actuators combined with a chamber exploiting the granular jamming mechanism.

The main component of the manipulator module is an elastomeric cylinder (silicone Ecoflex$^{\mathrm{TM}}$ 0050, Smooth-on Inc.). This material guarantees the right level of softness when deformed passively and it is suitable to host internal chambers that can be used to modulate the characteristics and the behavior of the module. The cylindrical elastomer hosts three equally spaced chambers which are embedded in radial arrangement (the fluidic actuators) and another one centrally placed (for granular jamming) as shown in

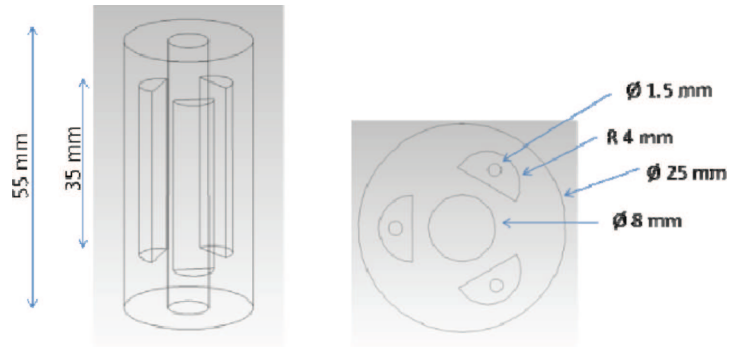

Figure 2.1 From left to right, sketch of the longitudinal and transversal cross section design of the module with the semicylindrical fluidic chambers and the central stiffening channel.

Figure 2.1. Externally the module is provided with a braided bellow-like structure.

2.1.1 Active Motion

Flexible fluidic actuators have been already successfully used as an active motion system enabling elongation and bending of soft structures [1]. The use of such technology is eased by the widely available literature in terms of modelization [2, 3] and application cases [4].

Optimal geometries for this specific system are under investigation, but previous works comparing several cross section designs for similar applications [5] concluded that the key factor is to find a trade-off between the thickness of the separation wall among the chambers and their diameter. Moreover, in this case an additional criterion is the maximization of the available internal space to host the stiffening chamber.

A well-known drawback on the use of soft material chambers inflated by pressurized fluids is the difficulty to have deformations along preferential directions to obtain bending and elongation. This is due to the fact that the inflated chambers tend to expand in every direction, like balloons. In Figure 2.2, the effect of 0.32 bar pressure on one chamber is shown and it is evident that the outward expansion is dominant with respect to the bending of the module and it reaches an unacceptably high risk of explosion.

On the contrary, in order to produce a more pronounced bending effect with minimal lateral expansion, the radial expansion of the chamber should

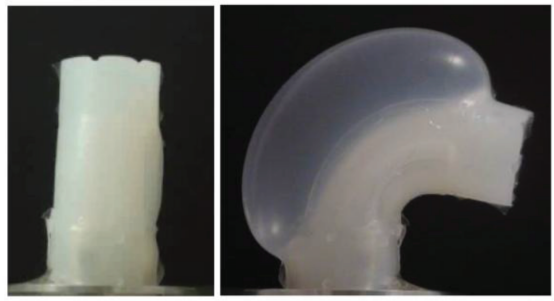

Figure 2.2 Effect of 0.32 bar pressure on a single silicone (Ecoflex 0050) chamber.

be minimized inducing a maximal longitudinal deformation. Since the elastomeric materials are considered isotropic, there are no preferential directions of expansion; however, adding other structures (fillers or external constrains) would force the elongation or the bending, limiting the diameter expansion and changing the overall module behavior.

Previous attempts to limit this lateral expansion demonstrated that circular fibers arranged all around the structure can serve the scope [6], but as the chamber deforms, the coils start to separate, leaving weaker areas on the external surface that could likely cause abrupt and dangerous lateral expansions. This risk is especially high if the elastomeric material is very soft and the achievable curvature is high. On the other hand, harder elastomers or a huge number of stiff fibers could compromise the performances of the manipulator or require a more powerful fluidic source.

Based on the above considerations, the main idea is to couple the silicone cylinder and its internal chambers with a braided structure (i.e., a sheath). Braided structures (like those used in the McKibben actuators) are highly flexible and can contemporarily follow bending and elongation movements providing a radial constraint to the excessive expansion especially if thermally formed to remain in a bellows-like shape.

The braided sheath is placed externally respect to the chambers and it is fixed at the distal ends of the cylinder. When the chambers are inflated to bend (or to elongate), the braided sheath contains and limits the radial expansion, thus maximizing the longitudinal effect of the deformation.

2.1.2 Stiffness variation

For stiffness modulation, a granular jamming solution is used. The effectiveness of this strategy on soft robots has been already demonstrated in [7–12].

One of the most interesting features of this technology is that it keeps a high deformability in the unjammed state and undergoes a drastic stiffness increase in the jammed condition. In our application, coffee powder was used as granular material and latex as containing membrane. Jamming transition is induced by increasing density in the flexible membrane due to the applied vacuum. By controlling the vacuum level the stiffness can be tuned.

2.2 Connection of Multiple Modules

The easiest strategy for module integration (in case of a limited number of modules) is based on the connection between the modules with pneumatic tubes that pass through the actuation chambers. This configuration allows aligning the chambers and having more free space within the module section.

A first prototype of the manipulator has been fabricated integrating three modules, designed on the basis of the approach reported in the previous section. The manipulator allowed evaluating the possible movements and optimizing the integration process for the fabrication of a second arm. This manipulator includes two modules and the geometry and dimensions of the single silicone unit are the same as that of the prototype illustrated in the previous section. The modules are connected with small silicone tubes passing through the chambers of the first module, as illustrated in Figure 2.3.

The connecting junction between two modules is the main element that has to be considered (length h in Figure 2.3). This area is not actuated and it does not include the granular jamming-based stiffening chamber. The junction connection has been designed in order to minimize its non-active effect on the system performance and not to prevail on that.

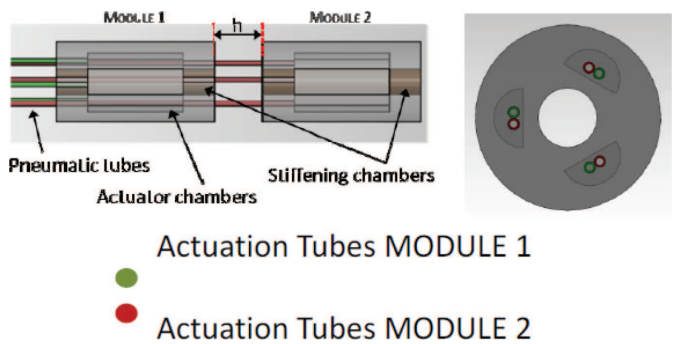

Figure 2.3 Overall view of the manipulator design (left) and bottom view (right).

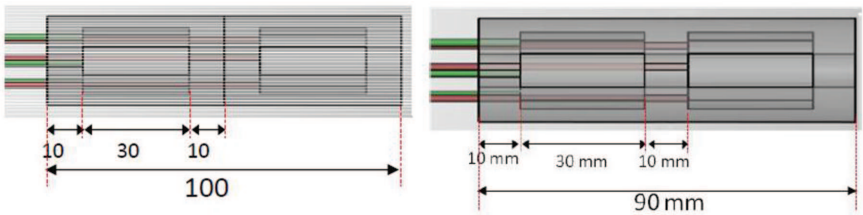

Figure 2.4 Theoretical length of the manipulator when two modules are connected (left) and manipulator with a junction of 10 mm (right).

If the manipulator is solicited laterally on the tip by a force, the designed configuration avoids a deflection of the manipulator in correspondence with the junction. In this way, it is guaranteed that, when evaluating the stiffening capabilities, the overall behavior of the manipulator will not be affected by the presence of this softer and non-active part. The theoretical length of the two-module manipulator is 100 mm which is twice the length of a single module as illustrated in Figure 2.4 (left).

The section between the modules has a length of 20 mm. However, 10 mm is sufficient for avoiding deformation of the silicone in the axial direction when it is inflated (see Figure 2.4, right panel). Therefore, a single junction of 10 mm has been designed between the chambers of the modules that will be functional for both the lower and upper modules.

Taking into account the geometry of the manipulator and the stiffness of the materials, an estimation of the junction displacement is given by:

$$y = \frac{Fh^3}{3EI} \tag{2.1}$$

where:

F is the applied force (N);

h is the junction length (m);

E is the elastic modulus of the junction (Pa);

I is the area moment of inertia (m^4) that is $\frac{\pi}{4}r^4$ for a filled circular area of radius r.

When a force is applied to the second module, the junction displacement can be controlled by dimensioning its length and material. The junction has been designed considering a small length of 8 mm and the material Dragon Skin 10 MEDIUM (Smooth-On) which is a silicone harder than Ecoflex 00-50 (Figure 2.5).

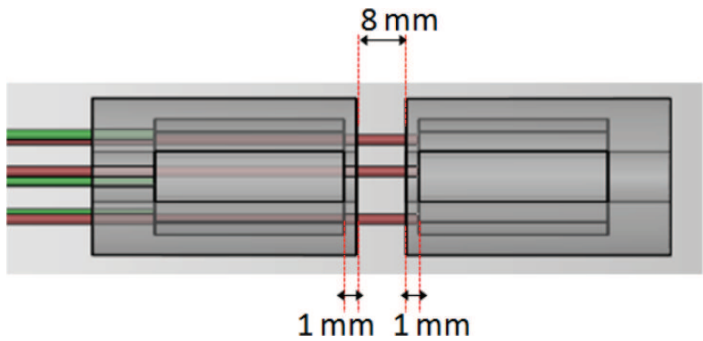

Figure 2.5 CAD of the junction zone.

For a force of 3 N, a length of 8 mm and a stiffness of 228 kPa (Dragon Skin), the displacement of the passive junction is:

$$y = \frac{3N \cdot (8mm)^3}{3 \cdot 228kPa \cdot \frac{\pi}{4} \cdot (12.5mm)^4} = 0.12mm \tag{2.2}$$

This displacement is negligible with respect to the displacement of the active unit, which is about 11 mm with a load force of 3 N as it is reported in Figure 2.6.

This configuration ensures a working length of 50 mm for each module and the effect of the junction is limited (see Figure 2.7).

In the 2-module manipulator the "in-series" stiffening mechanism has been inserted inside the central channel. Two membranes have been filled

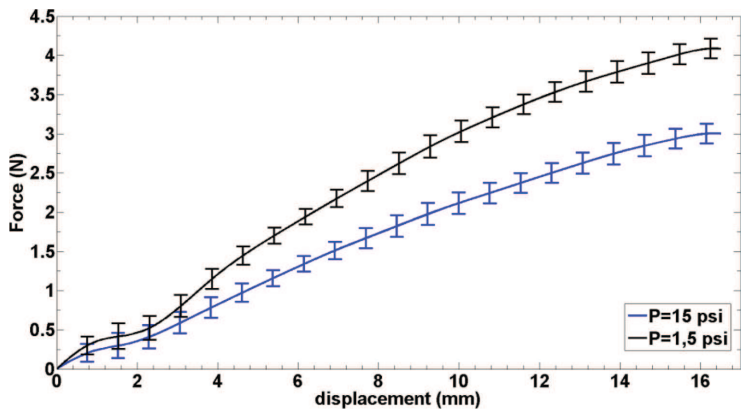

Figure 2.6 Force-displacement curve of the single module.

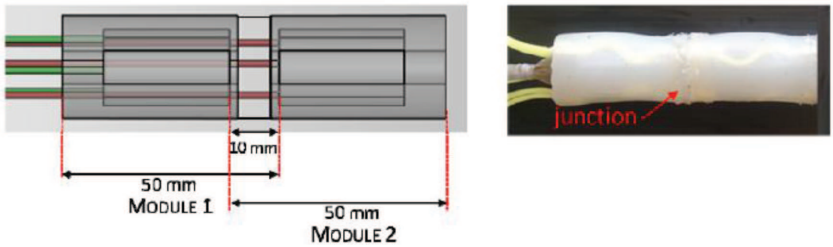

Figure 2.7 Final CAD of the 2-module manipulator (left) and the prototype (right).

Figure 2.8 Final prototype of the 2-module manipulator.

with 4 g of coffee grains and they have been connected with a tube of 4 mm diameter and 20 mm length. The vacuum has been applied simultaneously to the two membranes. Two external braided sheaths have been also integrated around the module. The final prototype is reported in Figure 2.8.

2.3 Complete Characterization of the 2-Module Manipulator

The soft manipulator is ideally composed of multiple modules, each one provided with actuation and stiffening capabilities. Starting from the design of the single module reported above and after the complete characterization of a single module reported in [13], we here extend the same analysis to a 2-module manipulator. This step is particularly significant since it allows—with a minimum number of modules—the testing of the combined performance of two interconnected modules in terms of stiffening and actuation.

The manipulator is composed of two connected identical modules, Figure 2.9. Each module possesses the original structure, with three fluidic chambers for the active omnidirectional motion combined with a central stiffening chamber, which exploits the granular jamming-based mechanism. This approach allows actuating and stiffening the modules independently.

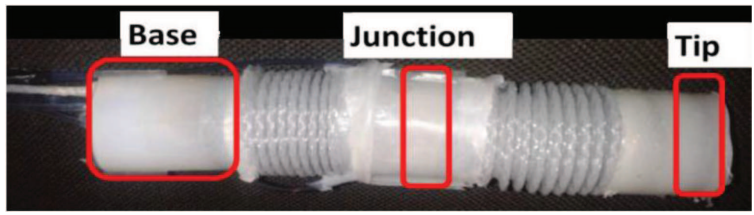

Figure 2.9 Fabricated 2-module manipulator.

2.3.1 Fabrication

The body of the module is fabricated by means of a molding process using Silicone (Silicone 0050, Ecoflex, *Smooth on Inc.*, Shore Hardness = 00-50, 100% linearized Tensile Modulus = 83 kPa). A crimped sheath is put around the module in order to contain the ballooning effect due to the chambers inflation. The detailed fabrication process of the module can be found in [13].

Each module incorporates a central channel for the granular jamming-based stiffening mechanism composed of an external latex membrane filled with 6 g of coffee; a 2 mm pipe is inserted inside and the membrane is sealed around it with Parafilm. The stiffening chamber is extended by approximately 0.5 cm on both sides with respect to the module length as shown in Figure 2.10a, top. This feature allows for keeping the stiffness variation

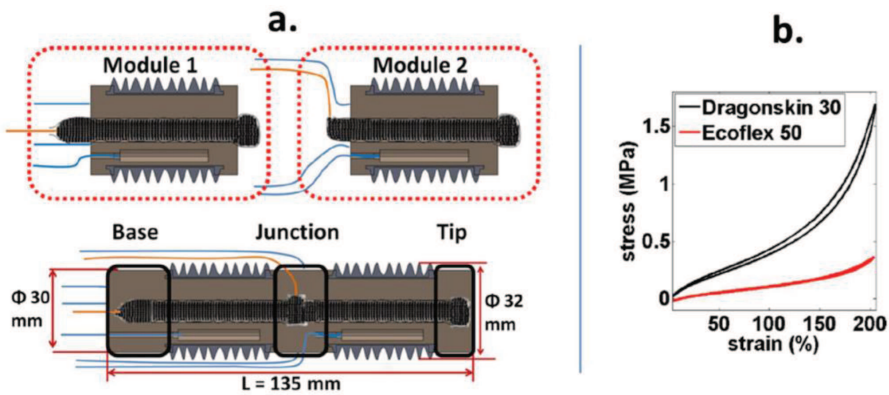

Figure 2.10 (a) Fabrication steps of the multi-module manipulator. Top, section of the two modules before connection. Bottom, two interconnected modules. In blue the pipes for the fluidic actuation; in orange the pipes for supplying vacuum to the stiffening chambers. The total length of the manipulator is given by the length of the two modules (50 mm), plus 10 mm of junction, 10 mm of the tip, and 15 mm on the base. (b) Experimental stress-strain curve of silicone rubbers according to ISO 37:2005(E).

capability even in the junction between the two modules by guaranteeing that the granular material will be present also in this section.

The pipes used both for inflating the fluidic chambers and for vacuuming the stiffening chamber are 2 mm outer diameter, 1.2 mm inner diameter polyurethane tubes (*SMC Corporation*). They are connected to the fluidic chambers after the fabrication of the modules. In order to avoid possible leakages, Sil-Poxy silicone rubber adhesive (*Smooth-on Inc.*) is used to glue them in the silicone channel used for supplying air to the fluidic chambers. In order to increase the adhesion of the pipes, their tips are scratched with sandpaper.

The inter-module connection is constructed by positioning the modules at 1 cm distance, while keeping the fluidic chambers aligned. This implies that the parts of the stiffening chamber sticking out from the module's top and bottom are in contact and slightly compressed among each other.

Two half-cylindrical shells with an inner diameter of 32 mm are then used to cap the junction and Silicone (Silicone 30, Dragonskin, Smooth on Inc., Hardness = 30, 100% linearized Tensile Modulus = 593 kPa) is poured inside. The same procedure is repeated at the top and the bottom of the manipulator, in order to fully close the structure (Figure 2.10a, bottom). The base is extended by 1.5 cm in order to simplify the clamping of the manipulator during the testing phase.

The use of a stiffer silicone material in the passive parts and particularly in the junction area guarantees that they do not affect the overall behavior of the manipulator. Dragonskin 30 silicone was chosen since it presents a stiffness 7 times higher than Ecoflex 0050 which is used for the fabrication of the modules. The mechanical properties of the two silicones were tested according to ISO 37:2005(E) and the stress-strain data are shown in Figure 2.10b. The curves of Figure 2.10b represent the average of five cycles of loading/unloading of the silicone performed with an Instron 5900 Testing System. The maximum measured variability was ± 3.4 kPa for the Ecoflex 0050 and 2.8 kPa for the Dragonskin 30.

2.3.2 Workspace Evaluation

The manipulator has been characterized through experimental tests aimed at verifying its dexterity, stiffening capability, and possibility of exploiting stiffness variation during the application of forces.

2.3.2.1 Methods

The actuation of the 2-module manipulator was performed by controlling the pressure in each fluidic chamber independently. Six proportional pressure regulator valves (series K8P, E.V.P. systems) were used to modulate the air pressure inflated in each chamber from 0.0 to 0.065 MPa (inset of Figure 2.11a). A compressor (Compact 106, Fiac Air-Compressors) was used as pneumatic air source. Vacuum for stiffness modulation was obtained by a vacuum regulator (ITV0090, SMC Corporation), shown in the inset of Figure 2.11a, and a vacuum pump (LB.4, D.V.P. Vacuum Technology).

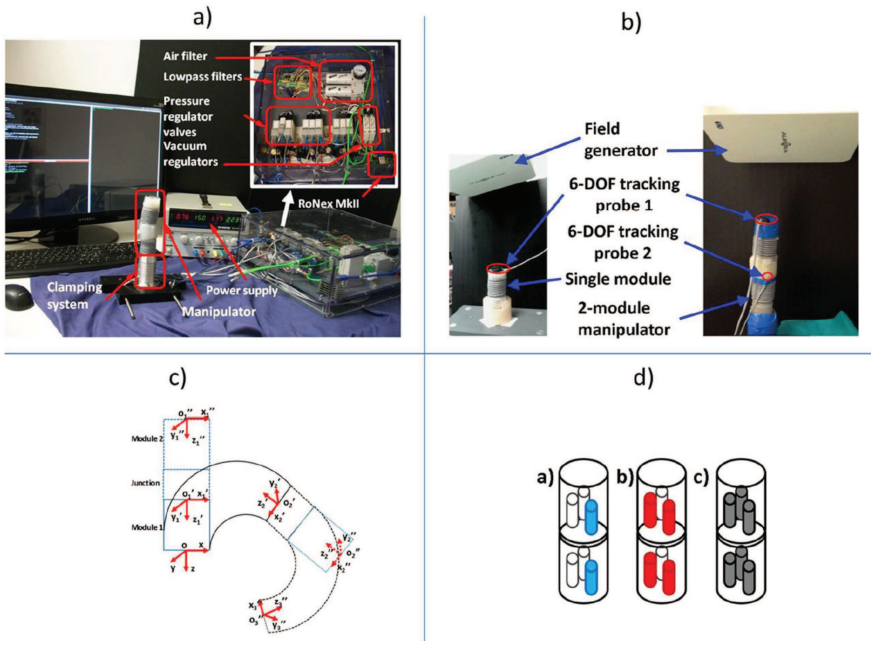

Figure 2.11 (a) Setup for the active motion and stiffening of the 2-module manipulator. In the inset the top view of the box is shown, indicating all components used for the control of the pneumatic actuation and of the vacuum levels. (b) Left, setup for the experimental measurement of the workspace of the single module. Right, setup used for the experimental measurement of specific configurations of the 2-module manipulator. The 6 DoF localization probe (Northern Digital Inc.) is highlighted in red in the pictures. (c) Scheme of the extrapolation strategy for computing the workspace of the 2-module manipulator from the workspace of the single module. The global coordinate system is o, the local coordinate system of the first module is o' and the local coordinate system of the second module is o''. (d) Scheme of the 2-module manipulator highlighting the chambers activated for single chamber bending (a), two chamber bending (b) and elongation (c).

The vacuum pump is able to provide a maximum vacuum of 0.03 Pa absolute pressure with a flow of 3 m^3/h. The vacuum generated inside the stiffening chamber was monitored with a pressure sensor (SWCN-V01-P3-2, Camozzi) and resulted in a maximum of –0.0987 MPa relative pressure. A 5 μm filter (MC104-D10, E.V.P. Systems) was used to prevent particles from entering the pump. The control of the pressure and vacuum regulators is done with low-pass filtered PWM signals generated from the digital I/O pins of the RoNex MkII (http://www.shadowrobot.com/products/ronex/).

The pressure within each chamber can be regulated by setting the period and the ON-time of the PWM signal for each pin. The RoNex MkII is programmed using the Robot Operating System (ROS). The components for the control of the manipulator are illustrated in Figure 2.11a. During the tests, the manipulator was fixed with a clamping system, as shown in Figure 2.11a.

The workspace of the 2-module manipulator was estimated through extrapolation from the single module one. The workspace of the single module was obtained by placing a 6-DOF probe (Northern Digital Inc.) on the tip of a single module and measuring the position and orientation of the tip at all the different pressure combinations in the three fluidic chambers (Figure 2.11b, left). The pressure tested in the chambers was varied from 0.0 to 0.065 MPa. Since the module motion in response to the applied pressure is not linear, the following pressures were tested, [0.00, 0.025, 0.035, 0.045, 0.050, 0.065] MPa. These pressures were experimentally found to significantly describe the motion of the module in previous works. All the different combinations of the aforementioned pressures were applied in the three chambers, thus realizing 63 combinations (i.e., 216 points). Each pressure combination was automatically set by the control system in ROS; between two pressure combinations the pressure was reset to 0.0 MPa in all the chambers. During the application of each combination of pressures, the position and orientation of the module tip were acquired with the Aurora® EM Tracking system for 1 s (i.e., 100 samples).

The workspace of the 2-module manipulator was computed from such data by considering, for each point reached from the tip of the first module, all the possible configurations of the second one. In Figure 2.11c, the procedure is shown in an exemplified scenario; the coordinate system o is the global coordinate system. The localization probe measures the position and orientation of the coordinate system o′ for each point of the workspace of the single module (with the Aurora tracking system).

The transformation matrices from the coordinate system o to o′ are computed from these experimental data. Assuming that the two modules composing the manipulator are identical, the two transformation matrices T01 (from global coordinates to first module tip) and T12 (from first module tip to second module tip) can be considered identical. The orientation and position of o″ (for every configuration) can be obtained by multiplying each T01 (one for every point of the first module workspace) for all the T01. The junction area is considered as an extra translation matrix in the local coordinate system o′. In Figure 2.11c, some explicative configurations of the system are drawn.

In configuration 1 (no actuation, rest condition), the position of the tip of the second module is obtained by a simple translation along the z1′ axis. When the first module is bent (configuration 2), applying the same transformation as before, the point o2″ can be obtained. Similarly, when even the second module would be bent, the same transformation that maps o into o2′ can be used on o2′ to obtain o3″.

Some relevant configurations of the manipulator, including elongation, bending with single-chamber actuation, and bending with 2-chamber actuation, were measured experimentally in order to assess the effectiveness of the behavior of the manipulator and compare it with the data obtained computationally by extending the workspace of the single module. Such measurements were performed by placing two 6-DOF probes on the manipulator, one at the tip and one at the end of the first module as shown in Figure 2.11b, right. In all cases the inflation pressures tested were [0.00, 0.025, 0.035, 0.045, 0.050, 0.065] MPa. In the case of single-chamber bending, one chamber of each module was inflated at the same time (Figure 2.11d, case a); for the 2-chamber bending, two chambers per module were pressurized by the same value and at the same time (Figure 2.11d, case b); for the elongation measurement all three chambers of the two modules were inflated by the same pressure at the same time (Figure 2.11d, case c).

2.3.2.2 Results

In Figure 2.12 the full workspace of the 2-module manipulator is shown. In Figure 2.12a, a section of the workspace is shown; the section cuts in two parts the workspace on the x-plane in order to have a clearer visualization. The initial position of the manipulator (no actuation) is schematically shown in the plot as a cylinder. The arc drawn by the points on the left side of Figure 2.12a corresponds to the single-chamber bending and is in agreement

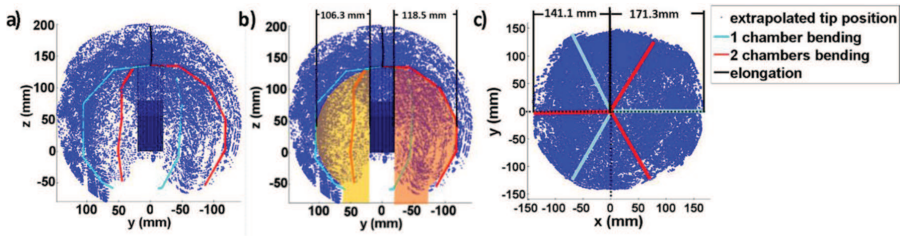

Figure 2.12 Workspace of the 2-module manipulator. (a) Section of the workspace along the x-plane, lateral view. (b) Section of the workspace with highlighted the unreachable areas. (c) Top view of the workspace.

with the results obtained with the single module in [13]; higher curvatures can be achieved and lower points in z direction can be reached (–75 mm with respect to the base of the manipulator). The right side of Figure 2.12a corresponds to the 2-chamber bending and presents a bigger radius of curvature. The experimental trajectories of the tip of the 2-module manipulator during single-chamber bending (cyan), 2-chamber bending (red) and elongation (black) match the extrapolated data. In Figure 2.12b the unreachable areas inside the workspace are highlighted; the yellow area is below the single-chamber bending and thus it extends slightly less than the red area, which is in correspondence with the 2-chamber bending. In Figure 2.12c the top view of the full workspace is reported. The planes corresponding to single- and 2-chamber bending are highlighted in cyan and red respectively. The system presented good symmetry properties (with 120° phase) in its behavior. The maximum diameter of a circle containing the whole workspace in the x-y plane (Figure 2.12c) is 312.4 mm.

In Figure 2.13 the results from the single- and 2-chamber bending are reported. Figures 2.13a and b represent the tip trajectories (position and orientation) of the manipulator during single- and 2-chamber bending respectively, together with a picture of the manipulator at the corresponding maximum reachable angle. In the plots of Figures 2.13a and b, the manipulator is reported in the non-actuated configuration as a cylinder and the trajectories, derived from the workspace extrapolation, are reported in blue, while the experimental data are in red. The two trajectories are very close for small pressures (around 0.04 MPa), but after that the error increases considerably, in particular along the z coordinate and especially for the 2-chamber bending trajectory. A very similar trend applies to the orientations (although the errors are smaller): the estimated bending angle is 236°±3.4° while the

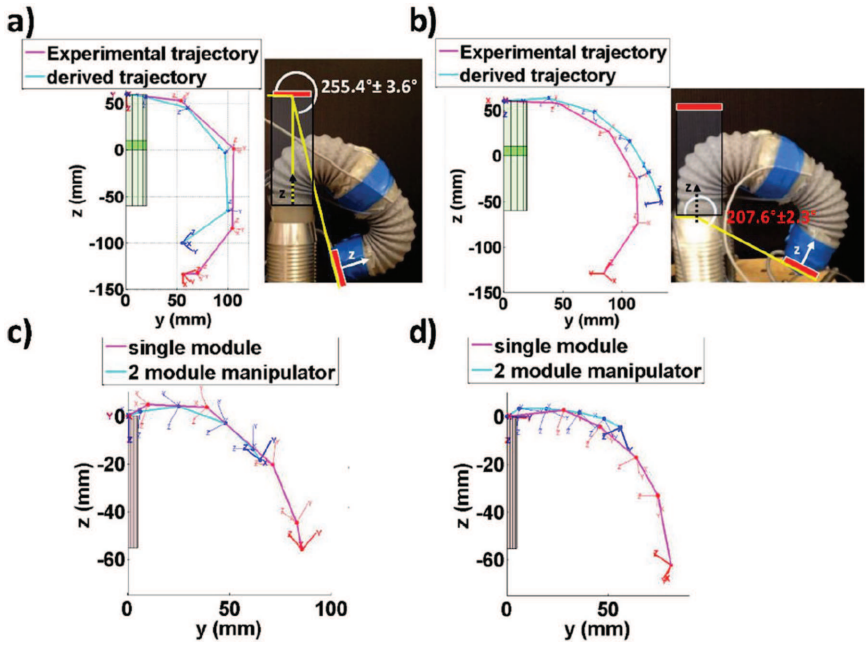

Figure 2.13 Comparison between experimentally measured trajectories end extrapolated ones. (a) Trajectories of the single-chamber bending in the 2-module manipulator and photo of the manipulator reaching the maximum bending angle with the single chamber inflation in both modules of 0.065 MPa. (b) Trajectories of the two chambers bending in the 2-module manipulator and a photo of the manipulator reaching the maximum bending angle with the 2-chamber inflation in both modules of 0.065 MPa. (c) Trajectory during single-chamber bending of a single module per se and when integrated in the 2-module manipulator. (d) Trajectory during two chamber-bending of a single module per se and when integrated in the 2-module manipulator.

measured one is 255°±3.6°. In the case of the 2-chamber bending, the computed bending angle is 175°±1.8° and the experimentally measured one is 207°±2.3°.

The possible reason for this difference can be found in Figures 2.13c and d where the trajectories of the single (Figure 2.13c) and 2-chamber (Figure 2.13d) bending, measured on a single manipulator (blue) and measured at the end of the first module of the 2-module manipulator (red) are reported. It is evident that the module is pushed down by the weight of the second module and this effect is higher at larger bending angles. In addition, the maximum bending angle with single-chamber bending of the

single module is 118°±3.2° while in the 2-module manipulator is 132°±2.9°. Similarly, the maximum bending angle with 2-chamber bending of the single module is 87.5°±1.8° while in the 2-module manipulator it is 115°±2.2°.

The experimental data suggest that the estimated workspace will present more points at the bottom in reality, but still it is a good approximation of the manipulator reachable space.

2.3.3 Junction Characterization

2.3.3.1 Methods

The mechanical properties of the junction area between the two modules were experimentally characterized using the setup shown in Figure 2.14. The active parts of the 2-module manipulator were fully constrained with two rigid shells and a fixed displacement was imposed to the tip of the manipulator by a 6 DOF industrial robot (RV-6SL, Mitsubishi) with an F/T sensor (MINI 45, ATI, USA, resolution = 0.025 N) fixed on its end effector. In this way the overall deflection was due only to the behavior of the junction area. The test was performed at different vacuum pressures in the stiffening chamber, i.e., 0.0 MPa, –0.052 MPa, and –0.098 MPa in both the stiffening chambers of the two modules; each test was repeated three times.

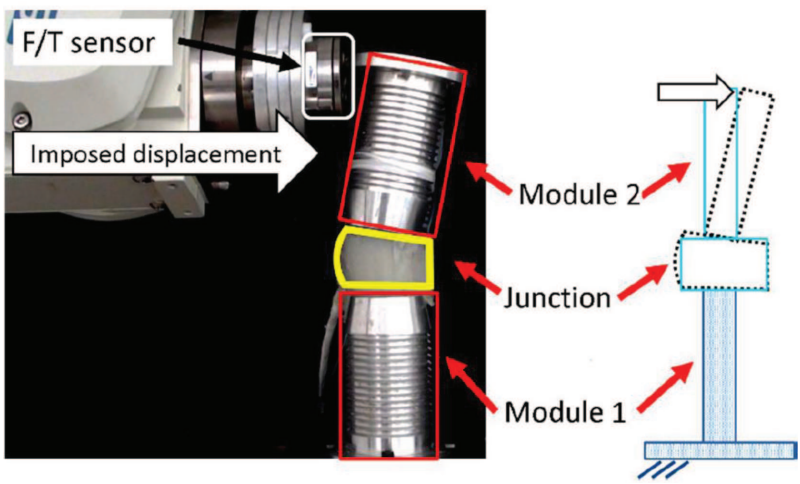

Figure 2.14 Setup for the experimental characterization of the junction are between the two modules. Left, assembled setup; in red the modules composing the manipulator are indicated, in yellow the deformed junction is highlighted. Right, scheme of the system.

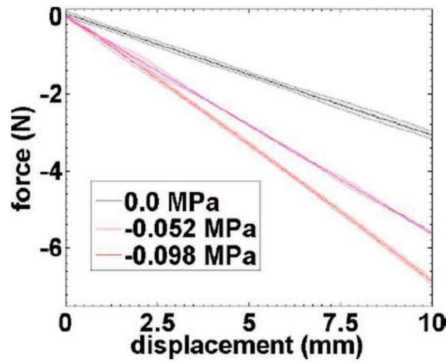

Figure 2.15 Results from the characterization of the junction between the two modules of the manipulator.

2.3.3.2 Results

In Figure 2.15, the results for the tests on the junction are reported. The forces necessary to deform the junction area reaches a maximum of 3.07±0.56 N at 10 mm displacement. Under the same conditions but applying –0.052 MPa pressure in the stiffening chambers, the force increases 5.61±0.08 N (83% increase) and reaches 6.86±0.12 N (123% increase) at –0.098 MPa. The slope of the curves (elastic constants) varies from 0.31 N/mm at atmospheric pressure to 0.54 N/mm at –0.052 MPa and 0.69 N/mm at –0.098 MPa.

2.3.4 Stiffness Characterization

2.3.4.1 Methods

The stiffening capabilities of the single module in different configurations in terms of bending and elongation have been extensively characterized in [13]. Here, the stiffening capabilities of the manipulator as a whole are presented. Tests were performed imposing different displacements at the tip of the manipulator by using a 6 DOF industrial robot (RV-6SL, Mitsubishi) with an F/T sensor (MINI 45, ATI, USA, resolution = 0.025 N ATI Mini45) fixed upon its end effector. In that way, it has been possible to impose the right orientation of the load cell respect to the module tip position. The same test was performed when the stiffening mechanism was not activated (0.1 MPa) and when –0.1 MPa vacuum was induced in the granular jamming-based stiffening mechanism; each test was repeated five times. The stiffness variation was characterized in both compression and tensile tests. Compression tests were performed compressing the manipulator along the z direction

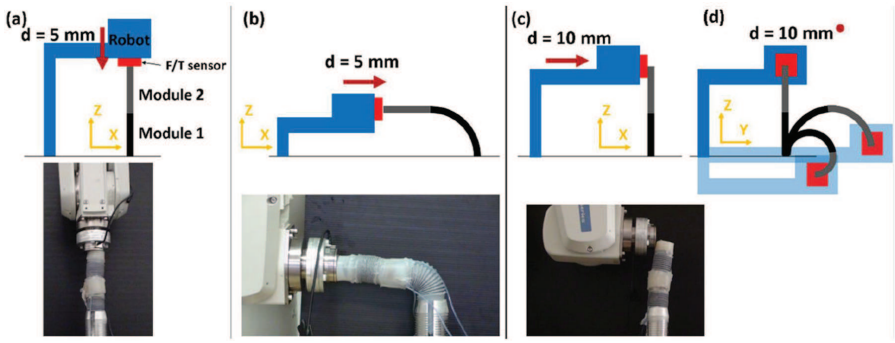

Figure 2.16 Manipulator configuration tested for evaluating the stiffening capabilities. The red square represents the F/T sensor, the blue structure represents the robot end effector; the base module of the manipulator is the black one and the second module is the dark gray one. (a) Axial test, (b) axial test with the first module 90° bent, (c) side view and (d) front view of the lateral test at different bending angles of the manipulator. For each configuration, the photo of the real setup is reported below.

(Figure 2.16a) of 5 mm. The same compression test was performed even when the first module is 90° bent (Figure 2.16b). Tensile tests were performed imposing a lateral displacement to the manipulator. Such tests were carried out both when the manipulator was in the fully straight configuration (Figure 2.16c) and at different bending angles (Figure 2.16d). The tests at different bending angles were performed inflating one chamber on each module with the same pressure; the tested pressures were [0.25, 0.35, 0.45, 0.55, 0.65] bar (Figure 16d).

2.3.4.2 Results

The results from the stiffness tests of Figure 2.16 are presented in Figure 2.17. The plots report the force measured from the F/T sensor with respect to the imposed displacement of the manipulator. Three different vacuum levels were applied to the stiffening chamber in order to verify the possibility of tuning the stiffness level. In Figure 2.17 (left) the results correspond to the configuration of Figure 2.16d. The force necessary to deflect the manipulator visibly changes according to the stiffening level. As an indication of the stiffness, the elastic constant was computed as the slope of the linear tract of the curves for the first 3 mm of displacement. The elastic constant varies from 0.11 N/mm when no stiffening is activated to 0.20 N/mm at –0.05 MPa vacuum pressure and up to 0.31 N/mm at –0.1 MPa.

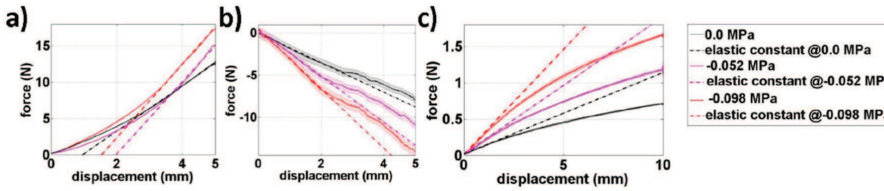

Figure 2.17 Results from the stiffness tests. (a) Axial tests. (b) Axial tests with the first module bent 90° (0.045 MPa inflation on one chamber). (c) Lateral test with no chamber inflation.

In Figure 2.17 (center) the results from the tests in the axial direction are reported (Figure 2.16a). In this case, for the first 2.5 mm displacement the effect of the stiffness variation is not evident. This is probably due to the change in volume of the stiffening chamber that tends to pack the granules together, thus leaving the tip with less granules and with a stiffness similar to the silicone one. On the other hand, it is possible to appreciate the stiffness variation when the displacement increases over 3 mm. In this case, the elastic constant was computed as the slope of the curves in the last part of the plot. The elastic constant varies from 2.18 N/mm when no stiffening is activated, up to 3.15 N/mm at –0.05 MPa vacuum pressure and 5.1 N/mm at –0.1 MPa.

Figure 2.17 (left) shows the results from the axial test when the first module is bent of 90° (Figure 2.16b). In this case the elastic constant varies from 1.99 N/mm when no stiffening is activated, to 2.6 N/mm at –0.05 MPa vacuum pressure, and 2.96 N/mm at –0.1 MPa. It is interesting to observe that the manipulator is able to withstand relatively high forces, also in the bent configuration; in particular, it withstood up to 17 N at –0.1 MPa vacuum pressure that is relevant for surgical tasks. In addition, these last curves presented a higher variability and a peak at around 3 mm. In fact, above a certain force, it starts to separate the jammed granules of the stiffening chamber and thus the performance of the stiffening mechanism decreases.

The results from all the stiffening tests are summarized in Table 2.1. The change in the elastic constant in the experiments was computed in the configurations shown in Figure 2.16. In the last column, the percentage of change in the stiffness is computed. It is important to observe that the stiffness variation is maintained also during the bending of the manipulator. As evident from Table 2.1, the elastic constant decreases due to the bending of the structure; however, the stiffening mechanism guarantees in all the configurations tested a considerable increase in the stiffness of the manipulator.

Table 2.1 Summary of the results from the stiffening tests on the 2-module manipulator

Test Typology	Chamber Inflation Pressure (bar)	Elastic Constant (N/mm) @ 0.1 MPa Pressure (Stiffening Chamber not Active)	Elastic Constant (N/mm) @ –0.1 MPa Pressure (Stiffening Chamber Active)	Elastic Constant Increase (%)
Lateral	0	0.11	0.31	66.6
	0.25	0.08	0.14	75
	0.35	0.05	0.15	200
	0.45	0.06	0.17	183,3
	0.55	0.06	0.17	183,3
	0.65	0.07	0.14	100
Axial	0	2.18	5.10	133.9
	0.45 @modulel	1.99	2.96	48.7

2.3.5 Combined Force and Stiffening Experiments

2.3.5.1 Methods

Two different types of tests were carried out to evaluate the forces exerted by the manipulator exploiting the selective stiffening capabilities of its segments. The first test consisted of positioning the manipulator in the same configuration as for the stiffening tests (Figure 2.16c). Three different vacuum levels ([0, –0.05, –0.1] MPa) were imposed in the first module (in black in Figure 2.8c) and the chamber of the second module that causes a bending on the x-z plane of Figure 2.16c was inflated at [0.25, 0.35, 0.45, 0.55, 0.65] bar. Forces were measured using an F/T sensor (ATI Nano17). The same procedure was performed while stiffening the second module and actuating the first one.

The second type of tests were aimed at exploiting the stiffening capabilities together with the possibility to generate forces in a more surgery-like scenario. Although the previously described tests provided a good overview of the 2-module manipulator, they still lack a thorough demonstration of the real capabilities of such a structure, in comparison with traditional rigid-link surgical manipulators.

For that reason, scenarios like that proposed in the schematic view of Figure 2.18 have been taken as guidelines to build a more reliable, credible test setup for the 2-module manipulator. To reproduce the compliance, in terms of weight and shape of organs or anatomical parts that the manipulator may encounter during surgical laparoscopic procedures, water-filled balloons have been employed and they have been placed around the manipulator to test its interaction with such objects.

Among the variety of possible tasks, a few key movements were chosen to demonstrate the manipulation and stiffening capabilities. These are the wrapping and retraction of a water-filled balloon (500 g, Figure 2.19a), hung

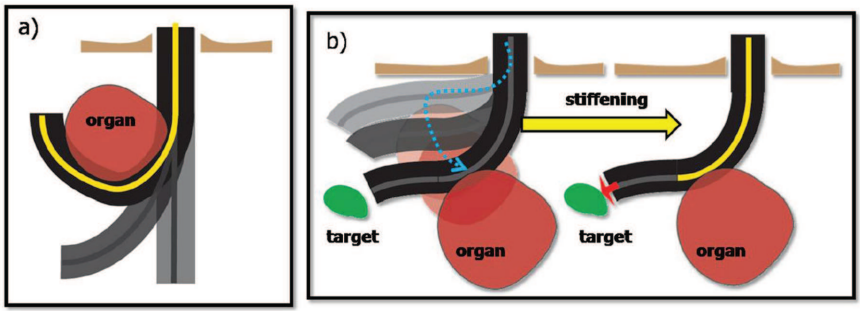

Figure 2.18 Schematic examples of surgical tasks performed by a tentacle-like structure. Left: organ retraction, showing the manipulator grabbing and lifting up of the organ. Right: fitting in tiny spaces, shifting down of an organ with the base portion, and reaching the surgical target with the distal module. The yellow line indicates the stiffening of the manipulator portion.

up to a load cell which revealed when the whole weight of the balloon was supported by the manipulator. Another task is shown in Figure 2.19 (center) where the manipulator navigates among compliant objects (water-filled balloons), embraces one of them (270 g), and moves it aside. The last

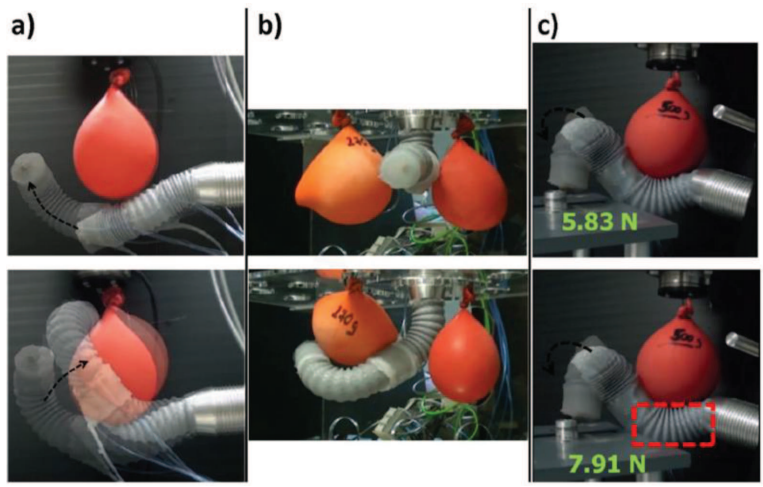

Figure 2.19 (a) the 2-module manipulator passes below a water filled balloon with the first module and exploits the second module to grasp and move the baloon around; (b) the manipulator fits between two water-filled balloons, lifting and shifting one of them to free access to the other one; (c) the manipulator is able to keep the weight of a 500 g balloon with the first module and apply a variable force on the F/T sensor.

task, presented in Figure 2.19 (right) demonstrated the manipulator supporting a weight of 500 g with the first module and applying a force on an F/T sensor. The same test is performed without stiffening activation and when the first module is fully stiffened. In this last experiment, two F/T sensors were used. One F/T sensor is connected to the water-filled balloon (5 N), while the other is positioned in the proximity of the distal end of the manipulator. In this test, two pieces of information can be extracted. The first F/T sensor allows verifying that the water filled balloon is completely supported, while the second F/T sensor measures the amount of force generated on the target.

2.3.5.2 Results

In Figure 2.20, the results from the combination of stiffening and actuation are presented. On the left the case when the stiffness of the base module is changed and the top module applies forces to the F/T sensor is shown. In this case the maximum force exerted when no stiffening is activated tends to saturate at approximately 1 N. On the other hand, when the base module is stiffened, the force is transmitted more effectively since it creates a more stable support for the second module when it applies force to the F/T sensor. The maximum force when the base module is fully stiffened reaches 2.2 N. This feature is important in order to apply force in a controlled way to tissues and biological structures. In the absence of stiffening capability, if the force necessary to shift a weight is too high, the structure may not succeed and may deform in an uncontrolled way in other directions due to its highly compliant structure.

The same test was performed by actuating the first module and changing the stiffness in the first one. In this case, the effect of the stiffness variation is not as effective as in the previous case. This is probably due to the fact

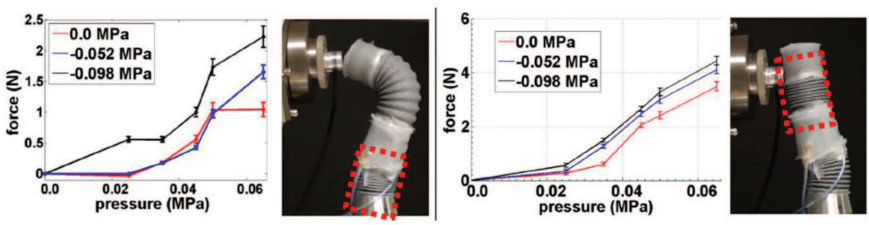

Figure 2.20 Results from the testing on the combination of actuation and stiffening. (Left) Stiffening of the base module, highlighted with the dashed square, and actuation of the first one. (Right) Stiffening of the second module (highlighted with the dashed square), and stiffening of the second one.

that the stiffening system is integrated in the central channel in order to keep the external compliance of the robot and thus its effect is mediated from the soft material in between. However, the maximum transmitted force increases from 3.45 to 4.47 N when the stiffening system is activated.

In Figure 2.19 some of the 2-module manipulators interacting with water-filled balloons are reported. In Figure 2.19c, in particular, the manipulator was able to keep the weight of a 500 g balloon with the first module and apply a force on the F/T sensor. The same test was performed when the first module was not stiffened and when it was stiffened. In the first case, the maximum recorded force was 5.83 N, in the second 7.91 N, thus validating the results obtained in Figure 2.19, left.

References

[1] Chang, B., Chew, A., Naghshineh, N., and Menon, C. (2012). A spatial bending fluidic actuator: fabrication and quasi-static characteristics. *Smart Mater. Struct*. 21:045008.

[2] Webster, R. J. III., and Jones, B. A. (2010). Design and kinematic modeling of constant curvature continuum robots: a review. *Int. J. Rob. Res*. 29, 1661–1683.

[3] Suzumori, K., Iikura, S., and Tanaka, H. (1991). "Flexible microactuator for miniature robots," in *Proceedings of the Micro Electro Mechanical Systems, MEMS '91, An Investigation of Micro Structures, Sensors, Actuators, Machines and Robots* (Nara: IEEE), 204–209.

[4] Greef, A. D., Lambert, P., and Delchambre, A., (2009). Towards flexible medical instruments: review of flexible fluidic actuators. *Precis. Eng*. 33, 311–321.

[5] Suzumori, K., Maeda, T., Watanabe, H., and Hisada, T. (1997). "Fiberless flexible microactuator designed by finite-element method," in *Proceedings of the IEEE/ASME Transactions on Mechatronics* (Roma: IEEE), 281–296.

[6] Suzumori, K., Endo, S., Kanda, T., Kato, N., and Suzuki, H. (2007). "A bending pneumatic rubber actuator realizing soft-bodied manta swimming robot," in *Proceedings of the IEEE International Conference on Robotics Automation 2007* (Roma: IEEE), 4975–4980.

[7] Cheng, N. G., Lobovsky, M. B., Keating, S. J., Setapen, A. M., Gero, K. I., Hosoi, A. E., et al. (2012). "Design and analysis of a robust, low-cost, highly articulated manipulator enabled by jamming of granular

media," in *Proceedings of the IEEE International Conference Robotics and Automation 2012 (ICRA)* (Saint Paul, MN: IEEE), 4328–4333.

[8] Brown, E., Rodenberg, N., Amend, J., Mozeika, A., Steltz, E., Zakin, M. R., et al. (2010). Universal robotic gripper based on the jamming of granular material. *Proc. Natl. Acad. Sci. U.S.A.* 107, 18 809–18 814.

[9] Steltz, E., Mozeika, A., Rembisz, J., Corson, N., and Jaeger, H. M. (2010). "Jamming as an enabling technology for soft robotics," in *Proceedings of the SPIE Conference on Electroactive Polymer Actuators and Devices 2010*, San Diego, CA.

[10] Loeve, A. J., van de Ven, O. S., Vogel, J. G., Breedveld, P., and Dankelman, J. (2010). Vacuum packed particles as flexible endoscope guides with controllable rigidity. *Granul. Matter* 12, 543–554.

[11] Jiang, A., Ataollahi, A., Althoefer, K., Dasgupta, P., and Nanayakkara, T. (2012). "A variable stiffness joint by granular jamming," in *Proceedings of the ASME 2012 International Design Engineering Technical Conferences and Computers and Information in Engineering Conference IDETC/CIE 2012*, Chicago, IL.

[12] Kaufhold, T., Bohm, V., and Zimmermann, K. (2012). "Design of a miniaturized locomotion system with variable mechanical compliance based on amoeboid movement," in *Proceedings of the 4th Biomedical Robotics and Biomechatronics (BioRob) 2012 IEEE RAS and EMBS International Conference on IEEE RAS* (Rome: IEEE), 1060–1065.

[13] Cianchetti, M., Ranzani, T., Gerboni, G., De Falco, I., Laschi, C., and Menciassi, A. (2013). "STIFF-FLOP surgical manipulator: mechanical design and experimental characterization of the single module," in *Proceedings of the IEEE/RSJ International Conference on Intelligent Robots and Systems*, Tokyo, 3576–3581.